Secondary organic aerosol formation from photochemical aging of light-duty gasoline vehicle exhausts in a smog chamber

Tengyu Liu[1,2], Xinming Wang[1,3,*], Wei Deng[1,2], Qihou Hu[1], Xiang Ding[1], Yanli Zhang[1], Quanfu He[1,2], Zhou Zhang[1,2], Sujun Lü[1,2], Xinhui Bi[1], Jianmin Chen[4], Jianzhen Yu[5]

1. State Key Laboratory of Organic Geochemistry, Guangzhou Institute of Geochemistry, Chinese Academy of Sciences, Guangzhou 510640, China
2. University of Chinese Academy of Sciences, Beijing 100049, China
3. Guangdong Key Laboratory of Environmental Protection and Resources Utilization, Guangzhou Institute of Geochemistry, Chinese Academy of Sciences, Guangzhou 510640, China
4. Shanghai Key Laboratory of Atmospheric Particle Pollution and Prevention, Department of Environmental Science & Engineering, Fudan University, Shanghai 200433, China
5. Division of Environment, Hong Kong University of Science & Technology, Clear Water Bay, Kowloon, Hong Kong, China

*Corresponding author:

Dr. Xinming Wang

State Key Laboratory of Organic Geochemistry

Guangzhou Institute of Geochemistry, Chinese Academy of Sciences

Tel: +86-20-85290180; Fax: +86-20-85290706

Email: wangxm@gig.ac.cn

Abstract

In China, fast increase in passenger vehicles has procured the growing concern about vehicle exhausts as an important source of anthropogenic secondary organic aerosols (SOA) in megacities hard-hit by haze. In this study, the SOA formation of emissions from two idling light-duty gasoline vehicles (LDGVs) (Euro 1 and Euro 4) operated in China was investigated in a 30 m^3 smog chamber. Five photo-oxidation experiments were carried out at 25 ℃ with the relative humidity around 50%. After aging at an OH exposure of 5×10^6 molecules cm^{-3} h, the formed SOA was 12–259 times as high as primary OA (POA). The SOA production factors (PF) were 0.001–0.044 g kg^{-1} fuel, comparable with those from the previous studies at comparable OH exposure. This quite lower OH exposure than that in typical atmospheric condition might however lead to the underestimation of the SOA formation potential from LDGVs. Effective SOA yield data in this study were well fit by a one-product gas-particle partitioning model and quite lower than those of a previous study investigating SOA formation from three idling passenger vehicles (Euro 2–Euro 4). Traditional single-ring aromatic precursors and naphthalene could explain 51%–90% of the formed SOA. Unspeciated species such as branched and cyclic alkanes might be the possible precursors for the unexplained SOA. A high-resolution time-of-flight aerosol mass spectrometer was used to characterize the chemical composition of SOA. The relationship between f_{43} (ratio of m/z 43, mostly $C_2H_3O^+$, to the total signal in mass spectrum) and f_{44} (mostly CO_2^+) of the gasoline vehicle exhaust SOA is similar

to the ambient semi-volatile oxygenated organic aerosol (SV-OOA). We plot the O:C and H:C molar ratios of SOA in a Van Krevelen diagram. The slopes of ΔH:C/ΔO:C ranged from -0.59 to -0.36, suggesting that the oxidation chemistry in these experiments was a combination of carboxylic acid and alcohol/peroxide formation.

1. Introduction

The formation mechanisms, magnitude and chemical composition of airborne fine particulate matter ($PM_{2.5}$) are important to evaluate its effects on human health and climate (Hallquist et al., 2009). Organic aerosol (OA) contributes roughly ~20% – 50% of the total fine particle mass at continental mid-latitudes (Saxena and Hildemann, 1996; Kanakidou et al., 2005). Atmospheric OA includes primary organic aerosol (POA) emitted from sources such as combustion of fossil fuels, biomass burning and volcanic eruptions, and secondary organic aerosol (SOA) formed via gas-particle conversion such as nucleation, condensation, and heterogeneous and multiphase chemistry or the aging of POA (Donahue et al., 2009; Jimenez et al., 2009). SOA is ubiquitous and dominates the total OA in various atmospheric environments, accounting for approximately two-thirds of the total OA in urban areas to almost 90% in urban downwind and rural areas in Northern Hemisphere mid-latitudes (Zhang et al., 2007). China, for example, has serious air quality problem due to $PM_{2.5}$ pollution in the recent decade (Chan and Yao 2008, Q. Zhang et al 2012), and SOA had contributed 30% – 90% of OA mass in its megacities (He et al., 2001; Cao et al., 2003; Duan et al., 2005, 2007; Yang et al., 2005; Hagler et al., 2006). However, models generally underestimate the observed OA levels mainly due to the unclear sources and formation processes of SOA (de Gouw et al., 2005; Heald et al., 2005; Johnson et al., 2006; Volkamer et al., 2006).

Vehicle exhausts emit plenty of primary PM and volatile organic compounds

(VOCs) containing precursors of SOA, influencing the near-surface atmospheric chemistry and the air quality, especially in urban areas. SOA formation from diesel generators and vehicles has been widely studied in smog chambers, demonstrating that the SOA mass formed from the exhaust of diesel generators and medium-, and heavy-duty diesel vehicles (HDDVs) usually exceeds the mass of emitted POA (Robinson et al., 2007; Weitkamp et al., 2007; Chirico et al., 2010; Miracolo et al., 2010; Samy and Zielinska, 2010; Nakao et al., 2011; Kroll et al., 2012). However, there are few studies on the SOA formation from gasoline vehicle exhausts. Nordin et al. (2013) investigated SOA formation from idling gasoline exhausts from three passenger vehicles (Euro 2 – Euro 4), finding that C_6-C_9 light aromatics contributed up to 60% of the formed SOA. While Platt et al. (2013) estimated aromatic precursors including C_6-C_{10} light aromatics and naphthalene were responsible for less than 20% of the SOA formed from the aging of emissions from a Euro 5 gasoline car operated during a New European Driving Cycle. To exclude the influence of a small sample size, Gordon et al. (2014) studied aging of emissions from 15 light-duty gasoline vehicles with model years ranging from 1987 to 2011, concluding that traditional precursors could fully explain the SOA from oldest vehicles and unspeciated organics were responsible for the majority of the SOA from the newer vehicles. Therefore, chemical compositions of SOA formed from gasoline vehicle exhaust varied a lot among vehicles with different types, model years and operating conditions.

In China, the number of LDGVs reached 98.8 million in 2012 and increased at a

rate of approximately 20% per year since 2005 (NBSC, 2013). Furthermore, gasoline fuel in China has relatively higher mass content of alkenes and aromatic hydrocarbons than that in US (Schauer et al., 2002; Zhang et al., 2013), and current emission standards of LDGVs in China lag behind European countries and US. The emission factors of $PM_{2.5}$, organic carbon (OC), element carbon (EC), NO_x, SO_2, NH_3 and non-methane hydrocarbons (NMHCs) for on-road vehicles in China were quite different from those in other countries (Liu et al., 2014; Y. L. Zhang et al., 2015). Therefore, it is urgent to investigate the SOA formation from vehicle exhaust in China to help make suitable policies to mitigate air pollution and also to provide valuable parameters to chemical transport models.

Here, we directly introduced dilute emissions from two idling light-duty gasoline vehicles (LDGVs) operated in China to a smog chamber to investigate the SOA formation. The magnitude and composition of the SOA formed from gasoline vehicle exhaust and whether traditional SOA precursors can explain the formed SOA was evaluated and discussed in this paper.

2. Materials and methods

2.1 Experimental setup

The photochemical aging experiments were carried out in the smog chamber in Guangzhou Institute of Geochemistry, Chinese Academy of Sciences (GIG-CAS). The GIG-CAS smog chamber has a 30 m^3 fluorinated ethylene propylene (FEP) reactor housed in a temperature-controlled room. Details of setup and facilities about the

chamber have been described elsewhere (Wang et al., 2014). Briefly, black lamps (1.2m-long, 60W Philips/10R BL, Royal Dutch Philips Electronics Ltd, The Netherlands) are used as light source, providing a NO_2 photolysis rate of 0.49 min^{-1}. Two Teflon-coated fans are installed inside the reactor to guarantee well mixing of the introduced gas species and particles within 120 seconds. Temperature can be set in the range from −10 to 40 °C at accuracy of ±1 °C as measured by eight temperature sensors inside the enclosure and one just inside the reactor. Relative humidity (RH) inside the reactor is achieved by vaporizing Milli-Q ultrapure water contained in a 0.5 L Florence flask and then flushing the water vapor into the reactor with purified dry air until target RH is reached. In the present study, temperature and RH inside the reactor were all set to 25 ℃ and 50%, respectively. During the experiments, the top frame is automatically lowered to maintain a differential positive pressure inside the reactor against the enclosure to avoid the contamination of the enclosure air.

Gasoline vehicle exhausts were injected to the reactor through Teflon lines using two oil-free pumps (Gast Manufacturing, Inc, USA) at a flow rate of 40 L min^{-1}. The injection time varied from a few minutes to more than one hour based on the primary emissions of different vehicles. A schematic of the smog chamber and the vehicle exhaust injection system is shown in Fig. 1.

2.2 Characterization of gas- and particle-phase chemical compositions and particle sizes

Gas-phase ozone (O_3) and NO_x were measured online with dedicated monitors

(EC9810 and 9841T, Ecotech, Australia). Online monitoring of parent VOCs such as C_6–C_{10} single-ring aromatic hydrocarbons and their oxidation products were available with a commercial proton-transfer-reaction time-of-flight mass spectrometer (PTR-TOF-MS, Model 2000, Ionicon Analytik GmbH, Austria). Detailed descriptions of the PTR-TOF-MS technique can be found elsewhere (Lindinger et al., 1998; Jordan et al., 2009). In this study the decay curve of toluene measured by PTR-TOF-MS were also used to derive the average hydroxyl radical (OH) concentration during each experiment. A wide spectrum of VOCs were also measured offline by drawing 250 ml air inside the reactor to a Model 7100 Preconcentrator (Entech Instruments Inc., USA) coupled with an Agilent 5973N gas chromatography-mass selective detector/flame ionization detector (GC-MSD/FID, Agilent Technologies, USA). Detailed descriptions of the method can be found elsewhere (Wang and Wu, 2008; Y. L. Zhang et al., 2010, 2012, 2013). C2-C3 and C4-C12 hydrocarbons were measured by GC-FID and GC-MSD, respectively. In this study, the offline measurement was the standard method to determine the mass concentrations of VOCs. PTR-TOF-MS was used for deriving the time-resolved concentrations of VOCs. The VOC concentrations measured offline were also used as an independent check of that measured online by the PTR-TOF-MS. To determine CO/ CO_2 concentrations before and after the introduction of exhausts, air samples were also collected into 2 L cleaned Teflon bags. CO was analyzed using a gas chromatography (Agilent 6980GC, USA) with a flame ionization detector and a packed column (5A Molecular Sieve 60/80 mesh, 3 m × 1/8

156 inch) (Y. L. Zhang et al., 2012), and CO_2 was analyzed with a HP 4890D gas
157 chromatography (Yi et al., 2007). The detection limits of CO and CO_2 were <30 ppb.
158 The relative SDs were all less than 3% based on 7 duplicates running 1.0 ppm CO and
159 CO_2 standards (Spectra Gases Inc, USA).

160 A high-resolution time-of-flight aerosol mass spectrometer (HR-TOF-MS,
161 Aerodyne Research Incorporated, USA) was used to measure the particle chemical
162 compositions (Jayne et al., 2000; DeCarlo et al., 2006). The instrument was operated
163 in the high sensitivity V-mode and high resolution W-mode alternatively every two
164 minutes. The toolkit Squirrel 1.51H was used to obtain time series of various mass
165 components (sulfate, nitrate, ammonium and organics). We used the toolkit Pika 1.1H
166 to determine the average element ratios of organics, like H:C, O:C, and N:C (Aiken et
167 al., 2007, 2008). The contribution of gas-phase CO_2 to the m/z 44 signal was
168 corrected using the measured CO_2 concentrations. The HR-TOF-MS was calibrated
169 using 300 nm monodisperse ammonium nitrate particles.

170 Particle number/volume concentrations and size distributions were measured
171 with a scanning mobility particle sizer (SMPS, TSI Incorporated, USA., classifier
172 model 3080, CPC model 3775). Flow rates of sheath and aerosol flow were 3.0 and
173 0.3 L min^{-1}, respectively, allowing a size distribution scanning ranging from 14 nm to
174 700 nm within 255 s. The accuracy of the particle number concentration is ±10%. An
175 aerosol density of 1.4 g cm^{-3} was assumed to convert the particle volume
176 concentration into the mass concentration (Zhang et al., 2005). Conductive silicon

177 tubes were used as sampling lines for HR-TOF-MS and SMPS to reduce electrostatic
178 losses of particles.

179 2.3 **Experimental procedure**

180 Two light-duty gasoline-powered vehicles were used in this study, one Euro 1 and one
181 Euro 4 vehicles. They are both port fuel injected vehicles. More details of the vehicles
182 are listed in Table 1. Both of the vehicles were fueled with Grade 93# gasoline, which
183 complies with the Euro III gasoline fuel standard. Details of the oil compositions can
184 be found in our previous study (Zhang et al., 2013).

185 Prior to each experiment, the reactor was evacuated and filled with purified dry
186 air for at least 5 times, then the reactor was flushed with purified dry air for at least 48
187 h until no residual hydrocarbons, O_3, NO_x, or particles were detected in the reactor to
188 avoid carry-over problems from day-to-day experiments. Prior to the introduction of
189 exhaust, the temperature control system and Teflon coated fans were turned on. The
190 exhaust could be injected when the temperature in the reactor was stable at the set
191 temperature 25 ℃.

192 The LDGV was parked outside the laboratory and tested at idling. Before the
193 injection of exhaust, the cars were at idling for at least half an hour to warm up the
194 three-way catalysts, and then the vehicle exhausts were injected into the reactor.
195 During the introduction, the raw exhausts were also sampled into 8 L cleaned
196 aluminum foil bags by a mechanical pump with a flow rate of about 5 L min^{-1}. VOCs
197 and CO_2 in these samples were measured offline by the same methods mentioned

198 above to characterize the primary emissions from the exhaust pipe. The exhaust in the
199 reactor was diluted by a factor of 13–30 compared to the tailpipe.

200 Additional NO was then added to adjust the VOC/NO_x ratios to around 10.0 or
201 2.0 (Table 2), within the range of 0.5–10 reported in gasoline vehicle exhaust tests and
202 downwind urban areas (Clairotte et al., 2013). The initial concentrations of NO_x at the
203 start of the experiments ranged from 134 to 956 ppb. In each experiment CH_3CN was
204 used as an indicator of dilution in the reactor. After being characterized in the dark for
205 more than 30 min, the exhaust was exposed to black light continuously for 5 h. After
206 the black lamps were switched off, the formed SOA was characterized for another 2 to
207 3 h to correct the particles wall loss. Blank experiments with no vehicle exhaust
208 introduced were performed to quantify the reactivity of the matrix gas. After 5 h of
209 irradiation, the number and mass of formed particles were <5 cm^{-3} and 0.1 μg m^{-3},
210 respectively.

211 During the introduction of exhausts, particles and VOCs might deposit to the
212 surface of the transfer lines. Therefore, a flow rate of as high as 20 L min^{-1} and a
213 transfer line of as short as 5 m were used to provide residence time within seconds,
214 and thus reduce the losses of particles and VOCs in the transfer lines. Furthermore,
215 before being introduced into the reactor, exhausts were generally pumped through the
216 transfer lines for half an hour to saturate the transfer lines with particles and VOCs
217 while warming the catalytic converter. Losses of particles and VOCs in the
218 introduction lines were determined by comparing the concentrations of total particle

number and VOCs in the directly emitted exhausts with the ones after passing through the transfer lines. The loss of total particle number was estimated to be less than 3%. The penetration efficiency of particles due to diffusion in a cylindrical tube, η(dp), can be also estimated by a laminar diffusional deposition model (Gormley and Kennedy, 1949). For particles with diameters larger than 10 nm, the penetration efficiency was higher than 95%, indicating minor losses of particles in the transfer line. The losses of VOCs in the transfer line were estimated to be less than 5%, which might lead to a small underestimation of SOA production.

2.4 Data analysis

2.4.1 Wall loss corrections

The loss of particles and organic vapors to the reactor walls has to be accounted for to accurately quantify the SOA formation. The loss of particles onto the walls has been well constrained and is treated as a first-order process (McMurry and Grosjean, 1985). The wall-loss rate constant was determined separately for each experiment by fitting the SMPS and AMS data with first-order kinetics when UV lamps were turned off. By applying this rate to the entire experiment, we use the same method as Pathak et al. (2007) treating the particle wall loss as a first order process to correct the wall loss of the particles. The wall loss of particles is a size-dependent process, therefore, the influence of nucleation need to be examined due to the rapid loss of nucleation mode particles. In this study, the impact of the nucleation event on wall-loss estimate is considered to be negligible for only less than 3% of the particle mass is in the

nucleation mode ten minutes after nucleation for all the experiments (Fig. S1 in the Supplement). In general, the loss of condensable organic vapors to the walls is estimated for two limiting cases (Weitkamp et al., 2007; Hildebrandt et al., 2009). In the first case (designated ω =0), no organic vapors is lost to the walls (only to suspended particles). In the second case (designated ω =1), the particles on the walls are in equilibrium with the organic vapors; therefore condensation to the particles on the walls is identical to the suspended particles. We use the ω =0 wall-loss correction assuming the organic vapors only condensation onto suspended particles. The ω =1 wall-loss correction is not suitable for the experiments here in which nucleation occurred and no seed particles were added (Henry et al., 2012).

2.4.2 AMS data corrections

Theoretically, the sum of the PM mass measured by AMS should be equal to the mass calculated from the SMPS mass size distributions. However, both methods have limitations. One must assume a particle shape and density to convert the volume concentration measured by SMPS to the mass concentration. Here, we assume that particles are spherical with an average density of 1.4 g cm^{-3} (Zhang et al., 2005). Fractal-like particles will cause the overestimate of the spherical equivalent diameter, thus overestimating the particle mass. AMS tends to underestimate the PM mass due to the transmission efficiency (Liu et al., 2007) and the AMS collection efficiency (Gordon et al., 2014), leading to the discrepancy between the AMS data and SMPS data. Fig. S2 shows the particle volume distribution measured by SMPS for a typical

smog chamber experiment (experiment 2). Most particles were in the range 40-120 nm after SOA formation. Since the transmission window of the standard lens of HR-TOF-AMS is 60-600 nm (aerodynamic diameter) (Liu et al., 2007), particles with diameter lower than 40 nm (mobility diameter) were cut from the lower edge of the volume distribution. After 1 h since nucleation occurred, only <5% of the mass was outside the transmission window of HR-TOF-MS, indicating that HR-TOF-AMS might underestimate the PM in the early stage of SOA formation. In this study, we use the same method as Gordon et al. (2014) to correct the AMS data.

For all the experiments with discrepancies between the AMS and SMPS data (Fig. S3), we assume that the difference in mass has the same composition as the measured components. We then calculate scaling factors, AMS_{sf}, to correct the PM mass measured by AMS and make it accordant with the SMPS measurements. The scaling factor is

$$AMS_{sf} = \frac{C_{SMPS}}{C_{Org} + C_{SO_4} + C_{NO_3} + C_{NH_4}} \quad (1)$$

where C_{SMPS} is the total particle mass concentration derived by the SMPS, C_{Org}, C_{SO4}, C_{NO3} and C_{NH4} are the mass concentrations of organics, sulfate, nitrate and ammonium measured by the AMS. As shown in Fig. S3, the mass of primary particles measured by SMPS was comparable with that measured by HR-TOF-AMS, thus we assumed that the mass of black carbon (BC) in the reactor was negligible. The AMS_{sf} for each time step after nucleation is calculated and used to scale the AMS data for the entire experiment.

2.4.3 Effective SOA yields

To compare the SOA formation with other studies, we calculated effective SOA yields for all experiments. The effective SOA yield Y was defined as the ratio of the wall-loss-corrected SOA mass to the mass of reacted organic precursors (Odum et al., 1996, 1997; Donahue et al., 2006). In this study, reacted organic precursors included in calculation are only those quantified by GC-MSD, including benzene, toluene, C2–benzene, C3–benzene, C4-benzene and naphthalene. A detailed list of these compounds is presented in Table S2. At the beginning and end of each experiment, air samples in the reactor were collected into 2 L electropolished and evacuated stainless steel canisters and analyzed by GC-MSD to determine the mass of reacted organic precursors.

2.4.4 Emission factors

Emission factor (EF) of a pollutant P is calculated on a fuel basis (g kg^{-1}):

$$EF = 10^3 \bullet [\Delta P] \bullet \left(\frac{MW_{CO_2}}{[\Delta CO_2]} + \frac{MW_{CO}}{[\Delta CO]} + \frac{MW_{HC}}{[\Delta HC]}\right) \bullet \frac{\omega_C}{MW_C} \quad (2)$$

where $[\Delta P]$, $[\Delta CO_2]$, $[\Delta CO]$, and $[\Delta HC]$ are the background corrected concentrations of P, CO_2, CO and the total hydrocarbons in the reactor in μg m^{-3}; MW_{CO2}, MW_{CO}, MW_{HC}, and MW_C are the molecular weights of CO_2, CO, HC and C. ω_C (0.85) is the carbon intensity of the gasoline (Kirchstetter et al., 1999).

2.4.5 Determination of OH exposure

Decay of toluene measured by PTR-TOF-MS is used to derive the average OH concentration during each experiment. Changes in the toluene concentration over time can be expressed as:

$$\frac{d[toluene]}{dt} = -k \cdot [OH] \cdot [toluene] \quad (3)$$

where k is the rate constant for the reaction between toluene and OH radical. Assuming a constant OH concentration during an experiment, we can integrate Eq. (3) to get Eq. (4):

$$\ln(\frac{[toluene]_0}{[toluene]_t}) = k \cdot [OH] \cdot t \quad (4)$$

So by plotting $ln([toluene]_0/[toluene]_t)$ versus time t, we can obtain a slope that equals $k \times [OH]$. The average OH concentration is therefore calculated as:

$$[OH] = \frac{slope}{k} \quad (5)$$

The OH exposure is then determined through multiplying the average OH concentration by time.

3. Results and discussion

3.1 VOC composition

Fig. 2 shows the average composition of gasoline vehicle exhausts from vehicle I (Euro 4) and II (Euro 1). For Euro 4 and 1 vehicle, alkanes contributed about 42.9% and 66.2% of the total speciated VOCs measured with the GC-FID/MSD by mass, respectively, dominating the speciated VOCs emissions in gasoline vehicle exhausts. Due to the high concentrations of isopentane and methylpentane, branched alkanes contributed approximately 44.9% of the total VOCs for Euro 1 vehicle, quite higher

than that for Euro 4 vehicle (23.3%). Aromatic hydrocarbons accounted for about 38.0% and 22.5% of the total VOCs for Euro 4 and 1 vehicle, respectively, relatively higher than 10-15% observed by Nordin et al. (2013) for idling Euro 2, 3 and 4 vehicles. The mass fraction of aromatic hydrocarbons for Euro 4 vehicle was comparable with 32.2% for idling private cars in Hong Kong (Guo et al., 2011) and 38.3% for Euro 3 light-duty gasoline vehicles operated through ECE cycles with an average speed around 18.7 km h^{-1} (Wang et al., 2013). Both Schauer et al. (2002) and Gentner et al. (2013) observed that aromatic hydrocarbons contributed around 27% of the total VOCs for gasoline-powered automobiles driven through the cold-start Federal Test Procedure urban driving cycle and on-road gasoline vehicles in the Caldecott tunnel, similar with that of Euro 1 vehicle. Recently, Huang et al. (2015) reported that mass fractions of aromatic hydrocarbons were as high as 46.4% for Euro 1, 2, and 3 light-duty gasoline vehicles operated through ECE cycles. Therefore, the variations of the composition of LDGV exhausts in this study were within the range of previous studies.

The averaged emission factors of VOCs and aromatic hydrocarbons for Euro 4 vehicle were 2.1 and 0.8 g kg^{-1}, approximately 26.0% and 43.5% of those for Euro 1 vehicle, respectively. Compared with a Euro 5 gasoline vehicle operated during a New European Driving Cycle, the emission factor of VOCs for Euro 4 vehicle was about 1.7 times higher (Platt et al., 2013). Using 7.87 L/100 km as the average fuel efficiency (Wagner et al., 2009), we obtained the VOCs emission factors based on g

343 km^{-1} for Euro 4 and 1 vehicles to be 0.12 and 0.46 g km^{-1}, respectively, comparable
344 with the previous reported values for Euro 1 and 4 gasoline vehicles in China (Huo et
345 al., 2012; Huang et al., 2015). According to previous studies, there is a clear reduction
346 of VOCs emissions from gasoline vehicles with stricter emission standards (Huo et al.,
347 2012; Huang et al., 2015). It is worth noting that emissions of HC from gasoline
348 vehicles during idling were observed to be lower than those in the acceleration and
349 deceleration modes (Tong et al., 2000; Yamamoto et al., 2012; Huang et al., 2013), but
350 in a similar level with those in the cruising mode (Tong et al., 2000). It is important to
351 note that the reported data are only based on five chamber experiments with two
352 LDGVs under idling conditions. More tests are needed to assess SOA formation from
353 gasoline vehicle exhausts in China.

354 **3.2 SOA formation**

355 Fig. 3 shows the temporal evolution of gas–phase and particle–phase species during a
356 typical smog chamber experiment. During -1.3 h to -0.85 h, the vehicle exhausts were
357 introduced into the reactor. At time = -0.55 h, the relative humidity was adjusted to
358 approximately 40%, and HR-TOF-AMS was connected to characterize the primary
359 PM. NO was injected to adjust the VOC/NO_x ratio at approximately time = -0.25 h.
360 After the black lamps were turned on, NO was fast converted to NO_2 in less than 1 h,
361 and then O_3 was accumulated and OH radical was formed. When NO concentration
362 decreased to a low level about 5 ppb, gas-phase light aromatics especially C_3–benzene
363 with higher reactivity, decayed rapidly due to the reaction with OH radical. SOA was

thus rapidly formed and increased to a high level in less than 2 h. As shown in Table 3, at the end of all the experiments, the formed SOA was 12–259 times as high as POA. This enhancement is consistent with 9–500 recently reported by Nordin et al. (2013) when studying SOA formation from idling European gasoline passenger vehicle emissions. As shown in Fig. 3c, the total particle number concentration increased fast from 82 to 116143 cm^{-3}, indicating dramatic new particle formation, which might be due to that the starting surface concentrations of particles were all below a critical value (100–2000 μm^2 cm^{-3}, Table S1) (Wehner et al., 2004). As shown in Table S1, primary particle numbers in the reactor in this study ranged from 82 to 18948 cm^{-3}, 1-2 orders of magnitude higher than that of a Euro 2 car operated at idling with a similar dilution ratio (Nordin et al., 2013), indicating that the small starting particle number concentrations might mainly due to the idling condition of tested cars rather than the losses in the introduction lines. In addition, upon entering into the chamber, emitted particles would partition due to dilution similar as in the atmosphere, regardless of the temperature and concentration in the sampling system, which might lead to the decrease of starting number concentrations. A certain extent of primary particles under the detection limit of 14 nm of SMPS also contributed to the measured small starting number concentration of particles.

Deposition of SOA-forming vapors to the walls might lead to the underestimation of SOA production. The wall loss rate coefficient of vapors is related with the numbers of carbon and oxygen in the molecule (X. Zhang et al., 2015). Here,

we take $C_7H_8O_4$, a product of the photo-oxidation of toluene as an example. The loss of $C_7H_8O_4$ to walls would be 7% in an hour before SOA formation when a wall deposition rate of 2×10^{-5} s^{-1} was used (X. Zhang et al., 2015). After SOA formation, the surface concentrations of particles increased fast to as high as 2000 μm^2 cm^{-3} in an hour, which would reduce the vapor wall losses.

SOA production factors (PF) for the LDGVs tested in this study were estimated to vary from 0.001 to 0.044g kg^{-1} fuel, which are within the results of Nordin et al. (2013) and Gordon et al. (2014) with OH exposure around 5.0×10^6 molecules cm^{-3} h. A recent study investigating SOA formation from in-use vehicle emissions in a highway tunnel in Pittsburg indicated that the peak SOA production was measured at an OH exposure of 1.9×10^8 molecules cm^{-3} h and current smog chamber studies may underestimate the ultimate SOA production by a maximum factor of about 10 due to the limited OH exposure (Tkacik et al., 2014).

The average OH radical concentration (Table 3) was determined to be 0.79-1.23 $\times10^6$ molecules cm^{-3} during our experiments. This OH level was about ten times lower than the average OH concentration of 1.5×10^7 molecules cm^{-3} around noon in summer in the Pearl River Delta, China (Hofzumahaus et al., 2009). The OH exposure in this study is only 5×10^6 molecules cm^{-3} h, equivalent to 0.3 hour of atmospheric oxidation. Therefore, the real-world SOA production factor from LDGVs in the atmosphere in China may be even higher than our estimation.

3.3 SOA yield

406 Effective SOA yield from vehicle exhaust calculated as described in 2.4.3 ranged
407 from 2.8% to 17.2%. Pankow (1994 a, b) and Odum et al. (1996) indicated that *Y* is a
408 function of M_0 and the relation is described as:

409 $$Y = M_0 \sum \left(\frac{\alpha_i K_{om,i}}{1 + K_{om,i} M_0}\right) \quad (6)$$

410 where $K_{om,i}$ and α_i are the mass-based absorption equilibrium partitioning coefficient
411 and stoichiometric coefficient of product *i*, respectively; M_0 is the total mass
412 concentration of organic material. As shown in Table 3, SOA yields for Euro 1 vehicle
413 were around 3%, quite lower than 10%-17% for Euro 4 vehicle. The mass fraction of
414 aromatic hydrocarbons for Euro 4 vehicle was about two times higher than that for
415 Euro 1 vehicle (Fig. 2a), which would form more semi-volatile organic compounds
416 (SVOCs) partitioning into particle phase under similar OH exposure and thus lead to
417 the relatively higher SOA yields.

418 Comparison of effective yield data obtained for the LDGV exhaust in this study
419 with those of Nordin et al. (2013) is shown in Fig. 4. Effective yield data of this study
420 are well fit with the one-product model, namely $Y = M_0\left(\frac{\alpha_1 K_{om,1}}{1+K_{om,1} M_0}\right)$. The
421 appropriate values for α_1 and $K_{om,1}$ when fitting the yields are 0.350 ± 0.114 and 0.007
422 ± 0.004, respectively. The effective SOA yields in the study of Nordin et al. (2013)
423 were 60%-360% higher than those in this study at same concentrations of M_0. In their
424 calculation of the reacted SOA precursors, C4-benzene and naphthalene were
425 excluded. The effective SOA yields would increase 7%-34% when C4-benzene and

naphthalene were excluded in this study, which could explain a small portion of the discrepancy. According to the estimation above, the loss of VOCs in the transfer lines was less than 5%. A little higher than VOCs, if assumed to be 20%, losses of IVOCs and SVOCs in the transfer lines would increase the SOA effective yields by a factor of 2%-10% when the unexplained SOA discussed later was all attributed to the contribution from IVOCs and SVOCs. The existence of seed particles in the study of Nordin et al. (2013) might reduce the wall loss of semi-volatile organic vapors and thus increase the effective SOA yield (Kroll et al., 2007; Zhang et al., 2014; X. Zhang et al., 2015). However, Cocker et al. (2001) found that SOA formation from m-xylene and 1,3,5-trimethylbenzene photo-oxidation was unaffected by the presence of ammonium sulfate seed aerosols. The influence of seed particles on SOA yields still needs further investigations. Faster oxidation rates caused by higher OH concentrations in the study of Nordin et al. (2013) would also result in higher SOA yields (Ng et al., 2007).Additionally, the different VOCs profiles of exhausts might also influence the SOA yields.

SOA production from the reacted organic precursors can be estimated by the following formula:

$$\Delta \mathrm{SOA}_{predicted} = \sum_{j} (\Delta X_j \times Y_j) \quad (7)$$

where $\Delta \mathrm{SOA}_{predicted}$ is the predicted SOA concentration in μg m^{-3}; ΔX_j is the mass of reacted aromatic hydrocarbon X_j in μg m^{-3}; and Y_j is the corresponding SOA yield of X_j. In this study, the SOA yield of benzene and other single-ring aromatics were

447 estimated using the two-product model curves taken from Borrás et al. (2012) and
448 Odum et al. (1997), respectively. While the SOA yield of naphthalene was taken from
449 Shakya et al. (2010). SOA yield curves of toluene and m-xylene from Ng et al. (2007)
450 were also widely used to estimate SOA production (Platt et al., 2013). However, the
451 introduction of seed aerosols and OH precursor made the SOA yield curves in the
452 study of Ng et al. (2007) not suitable for this study. Considering that the study of
453 Odum et al. (1997) provided a systematic estimation of SOA yields from toluene,
454 C2-benzene, C3-benzene and C4-benzene, we mainly used the two-product curves
455 from Odum et al. (1997) to estimate the SOA production. The aerosol yield curves
456 from literature were converted to the same aerosol density of 1.4 g cm^{-3} as this study.
457 The SOA yield for each precursor was calculated for the measured concentration of
458 OA in the reactor. Then the predicted SOA production from each precursor can be
459 calculated (Table S2).

460 Fig. 5 shows the contributions of the predicted benzene SOA, toluene SOA, C_2–
461 benzene SOA, C_3–benzene SOA, C_4–benzene SOA and naphthalene SOA to the total
462 measured SOA in all experiments. C_4–benzene contributed negligible SOA because of
463 the very low emissions of C_4–benzene from light-duty gasoline vehicles (Fig. 2b).
464 Though benzene took relatively higher percentage of the total VOCs, benzene also
465 accounted for a negligible proportion of the formed SOA due to its low reactivity with
466 OH radicals. Naphthalene was previously estimated to contribute around 5% of the
467 vehicle SOA mass (Nordin et al., 2013). While in this study naphthalene was

calculated to contribute 8%–52% of the formed SOA. The initial concentrations of naphthalene in this study ranged from 8.5 to 39.5 ppb, much higher than 2.8–4.4 ppb in the study of Nordin et al. (2013). The high contributions of naphthalene are probably attributed to its relatively higher initial concentrations and higher mass yield than single-ring aromatics for similar experimental conditions (Odum et al., 1997; Ng et al., 2007).

Totally, single-ring aromatics and naphthalene accounted for 51%–90% of the measured SOA, comparable to the estimation that classical C6–C9 light aromatics were responsible for 60% of the formed SOA from gasoline vehicle exhausts (Nordin et al., 2013), indicating that there are other SOA precursors in the LDGV exhausts. Platt et al. (2013) attributed the unexplained SOA formed from the aging of emissions from a Euro 5 gasoline car to highly oxygenated hydrocarbons. In addition, IVOCs such as branched and cyclic alkanes were recognized as important SOA precursors derived from wood burning, diesel engine and aircraft exhaust (Robinson et al., 2007; Weitkamp et al., 2007; Grieshop et al., 2009; Tkacik et al., 2012). Gordon et al. (2014) found that unspeciated species including branched and cyclic alkanes contributed about 30% of the nonmethane organic gas emissions from LDGVs with model years of 1995 or later and be associated with the majority of the SOA formation. Tkacik et al. (2014) also found that unspeciated species were predicted to contribute twice as much SOA from in-use vehicle emissions as traditional precursors. It is worth noting that photooxidation of aromatic hydrocarbons in a complex mixture such as gasoline

vehicle exhausts might alter the SOA yield compared to pure precursor experiments, thus probably influencing the estimation in this study (Song et al., 2007). Wall losses of organic vapors were not considered in this study, which would lead to the underestimation of SOA production. Therefore, the mass closure analysis estimated the maximum amount of SOA that could be explained by aromatics.

3.4 SOA composition

Fragmentations derived from the AMS data have been widely used to explore the oxidation degree of the organic aerosols (Zhang et al., 2005; Ng et al., 2010; Heald et al., 2010). The usually used ion fragments include m/z 43, 44 and 57. The dominating organic peaks in gasoline vehicle exhaust SOA are m/z 43 and 44 (Nordin et al., 2013), while m/z 57 is a main hydrocarbon fragment in diesel SOA (Chirico et al., 2010). Here, we use the approach of Ng et al. (2010) by plotting the fractions of total organic signal at m/z 43 (f_{43}) vs. m/z 44 (f_{44}) together with the triangle defined according to the analysis of ambient AMS data. The m/z 43 signal includes $C_3H_7^+$ and $C_2H_3O^+$ ions, indicating fresh less oxidized organic aerosols. The m/z 44 signal, dominated by CO_2^+ and formed from the thermal decarboxylation of organic acids, is an indicator of highly oxygenated organic aerosols (Ng et al., 2010).

Fig. 6a shows the f_{43} vs. f_{44} at the end of each experiment and the results of Nordin et al. (2013) and Presto et al. (2014), together with the triangle developed by Ng et al. (2010). The ambient low-volatility oxygenated OA (LV-OOA) and semi-volatile OOA (SV-OOA) factors fall in the upper and lower portions of the

510 triangle, respectively. Our data mainly lie in the SV-OOA region, similar to the results
511 of Nordin et al. (2013) and Presto et al. (2014). However, SOA in one experiment
512 show relatively lower oxidation degree. This phenomenon reflects the different SOA
513 compositions among different experiments and might be caused by the different
514 VOCs profiles, OH exposure and organic mass loadings (Ng et al., 2010).

515 The O:C ratio can also be used to characterize the oxidation degree of the
516 organic aerosols. After 5 h irradiation the H:C ratios varied from 1.22 to 1.37 and the
517 O:C ratios from 0.43 to 0.69 for all the experiments. Almost all the O:C values were
518 lower than 0.6, comparable to the SV-OOA compounds, which typically has O:C
519 ratios between 0.3 and 0.6 (Jimenez et al., 2009). Platt et al. (2013) observed a
520 relatively higher O:C ratio of 0.7 on the aging (OH = 12×10^{6} molecules cm^{-3} h) of
521 emissions from a Euro 5 gasoline car operated during a New European Driving Cycle.
522 As a higher OH exposure will lead to a higher O:C ratio, if the gasoline exhaust in this
523 study was irradiated under a similar OH exposure to that of Platt et al. (2013) , the
524 O:C ratios might reach to the similar level or higher, comparable to the LV-OOA
525 factor (Jimenez et al., 2009).

526 In Fig. 6b we plot the O:C and H:C molar ratios after SOA was formed during
527 experiments 1, 2 and 3 on a Van Krevelen diagram (Heald et al., 2010). The slopes
528 ranged from -0.59 to -0.36, similar to previous laboratory studies of Tkacik et al.
529 (2012) for cyclic, linear and branched alkanes, Jathar et al. (2013) for unburned fuel
530 and Presto et al. (2014) for light-duty gasoline vehicle exhaust. They are also similar

to the ambient data (Ng et al., 2011). A slope of -1, -0.5 and 0 in the Van krevelen diagram represents the addition of alcohol/peroxide, the addition of carboxylic acid with fragmentation, and the addition of carboxylic acid without fragmentation, respectively (Heald et al., 2010; Ng et al., 2011). Consequently, the slopes in this study indicate that the SOA formation is a combination of the addition of both carboxylic acid and alcohol/peroxide function groups without C-C bond cleavage and/or the addition of carboxylic acid with C-C bond breakage (Heald et al., 2010; Ng et al., 2011).

Acknowledgments

This study was supported by National Natural Science Foundation of China (Project No. 41025012/41121063), Strategic Priority Research Program of the Chinese Academy of Sciences (Grant No. XDB05010200), NSFC-Guangdong Joint Funds (U0833003) and Guangzhou Institute of Geochemistry (GIGCAS 135 project Y234161001).

547 **References**

548 Aiken, A. C., DeCarlo, P. F., and Jimenez, J. L.: Elemental Analysis of Organic
549 Species with Electron Ionization High-Resolution Mass Spectrometry, Anal. Chem.,
550 79, 8350-8358, 10.1021/ac071150w, 2007.
551 Aiken, A. C., DeCarlo, P. F., Kroll, J. H., Worsnop, D. R., Huffman, J. A., Docherty, K.
552 S., Ulbrich, I. M., Mohr, C., Kimmel, J. R., Sueper, D., Sun, Y., Zhang, Q.,
553 Trimborn, A., Northway, M., Ziemann, P. J., Canagaratna, M. R., Onasch, T. B.,
554 Alfarra, M. R., Prevot, A. S. H., Dommen, J., Duplissy, J., Metzger, A.,
555 Baltensperger, U., and Jimenez, J. L.: O/C and OM/OC ratios of primary, secondary,
556 and ambient organic aerosols with high-resolution time-of-flight aerosol mass
557 spectrometry, Environ. Sci. Technol., 42, 4478-4485, 10.1021/es703009q, 2008.
558 Borrás, E., and Tortajada-Genaro, L. A.: Secondary organic aerosol formation from
559 the photo-oxidation of benzene, Atmos. Environ., 47, 154-163, 2012.
560 Cao, J. J., Lee, S. C., Ho, K. F., Zhang, X. Y., Zou, S. C., Fung, K., Chow, J. C., and
561 Watson, J. G.: Characteristics of carbonaceous aerosol in Pearl River Delta Region,
562 China during 2001 winter period, Atmos. Environ., 37, 1451-1460, Doi
563 10.1016/S1352-2310(02)01002-6, 2003.
564 Chan, C. K., and Yao, X.: Air pollution in mega cities in China, Atmos. Environ., 42,
565 1-42, http://dx.doi.org/10.1016/j.atmosenv.2007.09.003, 2008.
566 Chirico, R., DeCarlo, P. F., Heringa, M. F., Tritscher, T., Richter, R., Prévôt, A. S. H.,
567 Dommen, J., Weingartner, E., Wehrle, G., Gysel, M., Laborde, M., and
568 Baltensperger, U.: Impact of aftertreatment devices on primary emissions and

569 secondary organic aerosol formation potential from in-use diesel vehicles: results
570 from smog chamber experiments, Atmos. Chem. Phys., 10, 11545-11563,
571 10.5194/acp-10-11545-2010, 2010.
572 Clairotte, M., Adam, T. W., Zardini, A. A., Manfredi, U., Martini, G., Krasenbrink, A.,
573 Vicet, A., Tournie, E., and Astorga, C.: Effects of low temperature on the cold start
574 gaseous emissions from light duty vehicles fuelled by ethanol-blended gasoline,
575 Appl. Energ., 102, 44–54, 2013.
576 Cocker Iii, D. R., Mader, B. T., Kalberer, M., Flagan, R. C., and Seinfeld, J. H.: The
577 effect of water on gas–particle partitioning of secondary organic aerosol: II.
578 m-xylene and 1,3,5-trimethylbenzene photooxidation systems, Atmos Environ, 35,
579 6073-6085, http://dx.doi.org/10.1016/S1352-2310(01)00405-8, 2001.
580 de Gouw, J. A., Middlebrook, A. M., Warneke, C., Goldan, P. D., Kuster, W. C.,
581 Roberts, J. M., Fehsenfeld, F. C., Worsnop, D. R., Canagaratna, M. R., Pszenny, A.
582 A. P., Keene, W. C., Marchewka, M., Bertman, S. B., and Bates, T. S.: Budget of
583 organic carbon in a polluted atmosphere: Results from the New England Air
584 Quality Study in 2002, J. Geophys. Res., 110, D16305, 10.1029/2004JD005623,
585 2005.
586 DeCarlo, P. F., Kimmel, J. R., Trimborn, A., Northway, M. J., Jayne, J. T., Aiken, A.
587 C., Gonin, M., Fuhrer, K., Horvath, T., Docherty, K. S., Worsnop, D. R., and
588 Jimenez, J. L.: Field-Deployable, High-Resolution, Time-of-Flight Aerosol Mass
589 Spectrometer, Analytical Chemistry, 78, 8281-8289, 10.1021/ac061249n, 2006.

590 Donahue, N. M., Robinson, A. L., Stanier, C. O., and Pandis, S. N.: Coupled
591 partitioning, dilution, and chemical aging of semivolatile organics, Environ. Sci.
592 Technol., 40, 2635-2643, 10.1021/es052297c, 2006.
593 Donahue, N. M., Robinson, A. L., and Pandis, S. N.: Atmospheric organic particulate
594 matter: From smoke to secondary organic aerosol, Atmos. Environ., 43, 94-106,
595 http://dx.doi.org/10.1016/j.atmosenv.2008.09.055, 2009.
596 Duan, F. K., He, K. B., Ma, Y. L., Jia, Y. T., Yang, F. M., Lei, Y., Tanaka, S., and
597 Okuta, T.: Characteristics of carbonaceous aerosols in Beijing, China, Chemosphere,
598 60, 355-364, DOI 10.1016/j.chemosphere.2004.12.035, 2005.
599 Duan, F. K., Liu, X. D., He, K. B., Li, Y. W., and Dong, S. P.: Characteristics and
600 source identification of particulate matter in wintertime in Beijing, Water Air Soil
601 Poll, 180, 171-183, DOI 10.1007/s11270-006-9261-4, 2007.
602 Gentner, D. R., Worton, D. R., Isaacman, G., Davis, L. C., Dallmann, T. R., Wood, E.
603 C., Herndon, S. C., Goldstein, A. H., and Harley, R. A.: Chemical Composition of
604 Gas-Phase Organic Carbon Emissions from Motor Vehicles and Implications for
605 Ozone Production, Environ. Sci. Technol., 47, 11837-11848,
606 doi:10.1021/es401470e, 2013.
607 Gordon, T. D., Presto, A. A., May, A. A., Nguyen, N. T., Lipsky, E. M., Donahue, N.
608 M., Gutierrez, A., Zhang, M., Maddox, C., Rieger, P., Chattopadhyay, S.,
609 Maldonado, H., Maricq, M. M., and Robinson, A. L.: Secondary organic aerosol
610 formation exceeds primary particulate matter emissions for light-duty gasoline

611 vehicles, Atmos. Chem. Phys., 14, 4661-4678, 10.5194/acp-14-4661-2014, 2014.
612 Gormley, P. G., and Kennedy, M.: Diffusion from a Stream Flowing through a
613 Cylindrical Tube, Proceedings of the Royal Irish Academy. Section A:
614 Mathematical and Physical Sciences, 52, 163-169, doi:10.2307/20488498, 1949.
615 Guo, H., Zou, S. C., Tsai, W. Y., Chan, L. Y., and Blake, D. R.: Emission
616 characteristics of nonmethane hydrocarbons from private cars and taxis at different
617 driving speeds in Hong Kong, Atmos. Environ., 45, 2711-2721,
618 http://dx.doi.org/10.1016/j.atmosenv.2011.02.053, 2011.
619 Hagler, G. S., Bergin, M. H., Salmon, L. G., Yu, J. Z., Wan, E. C. H., Zheng, M., Zeng,
620 L. M., Kiang, C. S., Zhang, Y. H., Lau, A. K. H., and Schauer, J. J.: Source areas
621 and chemical composition of fine particulate matter in the Pearl River Delta region
622 of China, Atmos. Environ., 40, 3802-3815, DOI 10.1016/j.atmosenv.2006.02.032,
623 2006.
624 Hallquist, M., Wenger, J. C., Baltensperger, U., Rudich, Y., Simpson, D., Claeys, M.,
625 Dommen, J., Donahue, N. M., George, C., Goldstein, A. H., Hamilton, J. F.,
626 Herrmann, H., Hoffmann, T., Iinuma, Y., Jang, M., Jenkin, M. E., Jimenez, J. L.,
627 Kiendler-Scharr, A., Maenhaut, W., McFiggans, G., Mentel, T. F., Monod, A.,
628 Prévôt, A. S. H., Seinfeld, J. H., Surratt, J. D., Szmigielski, R., and Wildt, J.: The
629 formation, properties and impact of secondary organic aerosol: current and
630 emerging issues, Atmos. Chem. Phys., 9, 5155-5236, 10.5194/acp-9-5155-2009,
631 2009.

He, K., Yang, F., Ma, Y., Zhang, Q., Yao, X., Chan, C. K., Cadle, S., Chan, T., and Mulawa, P.: The characteristics of $PM_{2.5}$ in Beijing, China, Atmos. Environ., 35, 4959-4970, http://dx.doi.org/10.1016/S1352-2310(01)00301-6, 2001.

Heald, C. L., Jacob, D. J., Park, R. J., Russell, L. M., Huebert, B. J., Seinfeld, J. H., Liao, H., and Weber, R. J.: A large organic aerosol source in the free troposphere missing from current models, Geophys. Res. Lett., 32, L18809, 10.1029/2005GL023831, 2005.

Heald, C. L., Kroll, J. H., Jimenez, J. L., Docherty, K. S., DeCarlo, P. F., Aiken, A. C., Chen, Q., Martin, S. T., Farmer, D. K., and Artaxo, P.: A simplified description of the evolution of organic aerosol composition in the atmosphere, Geophys. Res. Lett., 37, L08803, 10.1029/2010gl042737, 2010.

Henry, K. M., Lohaus, T., and Donahue, N. M.: Organic Aerosol Yields from α-Pinene Oxidation: Bridging the Gap between First-Generation Yields and Aging Chemistry, Environ Sci Technol, 46, 12347-12354, 10.1021/es302060y, 2012.

Hildebrandt, L., Donahue, N. M., and Pandis, S. N.: High formation of secondary organic aerosol from the photo-oxidation of toluene, Atmos. Chem. Phys., 9, 2973-2986, 10.5194/acp-9-2973-2009, 2009.

Hofzumahaus, A., Rohrer, F., Lu, K., Bohn, B., Brauers, T., Chang, C.-C., Fuchs, H., Holland, F., Kita, K., Kondo, Y., Li, X., Lou, S., Shao, M., Zeng, L., Wahner, A., and Zhang, Y.: Amplified Trace Gas Removal in the Troposphere, Science, 324, 1702-1704, 10.1126/science.1164566, 2009.

653 Huang, C., Lou, D. M., Hu, Z. Y., Feng, Q., Chen, Y. R., Chen, C. H., Tan, P. Q., and
654 Yao, D.: A PEMS study of the emissions of gaseous pollutants and ultrafine
655 particles from gasoline- and diesel-fueled vehicles, Atmos Environ, 77, 703-710,
656 DOI 10.1016/j.atmosenv.2013.05.059, 2013.
657 Huang, C., Wang, H. L., Li, L., Wang, Q., Lu, Q., de Gouw, J. A., Zhou, M., Jing, S.
658 A., Lu, J., and Chen, C. H.: VOC species and emission inventory from vehicles and
659 their SOA formation potentials estimation in Shanghai, China, Atmos. Chem. Phys.
660 Discuss., 15, 7977-8015, 10.5194/acpd-15-7977-2015, 2015.
661 Huo, H., Yao, Z., Zhang, Y., Shen, X., Zhang, Q., Ding, Y., and He, K.: On-board
662 measurements of emissions from light-duty gasoline vehicles in three mega-cities
663 of China, Atmos. Environ., 49, 371-377, doi:10.1016/j.atmosenv.2011.11.005,
664 2012.
665 Jathar, S. H., Miracolo, M. A., Tkacik, D. S., Donahue, N. M., Adams, P. J., and
666 Robinson, A. L.: Secondary Organic Aerosol Formation from Photo-Oxidation of
667 Unburned Fuel: Experimental Results and Implications for Aerosol Formation from
668 Combustion Emissions, Environ Sci Technol, 47, 12886-12893,
669 10.1021/es403445q, 2013.
670 Jathar, S. H., Gordon, T. D., Hennigan, C. J., Pye, H. O. T., Pouliot, G., Adams, P. J.,
671 Donahue, N. M., and Robinson, A. L.: Unspeciated organic emissions from
672 combustion sources and their influence on the secondary organic aerosol budget in
673 the United States, Proceedings of the National Academy of Sciences, 111,

674 10473-10478, 10.1073/pnas.1323740111, 2014.
675 Jayne, J. T., Leard, D. C., Zhang, X., Davidovits, P., Smith, K. A., Kolb, C. E., and
676 Worsnop, D. R.: Development of an Aerosol Mass Spectrometer for Size and
677 Composition Analysis of Submicron Particles, Aerosol. Sci. Tech., 33, 49-70,
678 10.1080/027868200410840, 2000.
679 Jimenez, J. L., Canagaratna, M. R., Donahue, N. M., Prevot, A. S. H., Zhang, Q.,
680 Kroll, J. H., DeCarlo, P. F., Allan, J. D., Coe, H., Ng, N. L., Aiken, A. C., Docherty,
681 K. S., Ulbrich, I. M., Grieshop, A. P., Robinson, A. L., Duplissy, J., Smith, J. D.,
682 Wilson, K. R., Lanz, V. A., Hueglin, C., Sun, Y. L., Tian, J., Laaksonen, A.,
683 Raatikainen, T., Rautiainen, J., Vaattovaara, P., Ehn, M., Kulmala, M., Tomlinson, J.
684 M., Collins, D. R., Cubison, M. J., E., Dunlea, J., Huffman, J. A., Onasch, T. B.,
685 Alfarra, M. R., Williams, P. I., Bower, K., Kondo, Y., Schneider, J., Drewnick, F.,
686 Borrmann, S., Weimer, S., Demerjian, K., Salcedo, D., Cottrell, L., Griffin, R.,
687 Takami, A., Miyoshi, T., Hatakeyama, S., Shimono, A., Sun, J. Y., Zhang, Y. M.,
688 Dzepina, K., Kimmel, J. R., Sueper, D., Jayne, J. T., Herndon, S. C., Trimborn, A.
689 M., Williams, L. R., Wood, E. C., Middlebrook, A. M., Kolb, C. E., Baltensperger,
690 U., and Worsnop, D. R.: Evolution of Organic Aerosols in the Atmosphere, Science,
691 326, 1525-1529, 10.1126/science.1180353, 2009.
692 Johnson, D., Utembe, S. R., Jenkin, M. E., Derwent, R. G., Hayman, G. D., Alfarra,
693 M. R., Coe, H., and McFiggans, G.: Simulating regional scale secondary organic
694 aerosol formation during the TORCH 2003 campaign in the southern UK, Atmos.

695 Chem. Phys., 6, 403-418, 10.5194/acp-6-403-2006, 2006.
696 Jordan, A., Haidacher, S., Hanel, G., Hartungen, E., Mark, L., Seehauser, H.,
697 Schottkowsky, R., Sulzer, P., and Mark, T. D.: A high resolution and high sensitivity
698 proton-transfer-reaction time-of-flight mass spectrometer (PTR-TOF-MS), Int. J.
699 Mass Spectrom., 286, 122-128, 2009.
700 Kanakidou, M., Seinfeld, J. H., Pandis, S. N., Barnes, I., Dentener, F. J., Facchini, M.
701 C., Van Dingenen, R., Ervens, B., Nenes, A., Nielsen, C. J., Swietlicki, E., Putaud, J.
702 P., Balkanski, Y., Fuzzi, S., Horth, J., Moortgat, G. K., Winterhalter, R., Myhre, C.
703 E. L., Tsigaridis, K., Vignati, E., Stephanou, E. G., and Wilson, J.: Organic aerosol
704 and global climate modelling: a review, Atmos. Chem. Phys., 5, 1053-1123,
705 10.5194/acp-5-1053-2005, 2005.
706 Kirchstetter, T. W., Harley, R. A., Kreisberg, N. M., Stolzenburg, M. R., and Hering, S.
707 V.: On-road measurement of fine particle and nitrogen oxide emissions from light-
708 and heavy-duty motor vehicles, Atmos. Environ., 33, 2955-2968,
709 http://dx.doi.org/10.1016/S1352-2310(99)00089-8, 1999.
710 Kroll, J. H., Chan, A. W. H., Ng, N. L., Flagan, R. C., and Seinfeld, J. H.: Reactions
711 of Semivolatile Organics and Their Effects on Secondary Organic Aerosol
712 Formation, Environ Sci Technol, 41, 3545-3550, 10.1021/es062059x, 2007.
713 Kroll, J. H., Smith, J. D., Worsnop, D. R., and Wilson, K. R.: Characterisation of
714 lightly oxidised organic aerosol formed from the photochemical aging of diesel
715 exhaust particles, Environmental Chemistry, 9, 211-220,

716 http://dx.doi.org/10.1071/EN11162, 2012.
717 Lindinger, W., Hansel, A., and Jordan, A.: On-line monitoring of volatile organic
718 compounds at pptv levels by means of proton-transfer-reaction mass spectrometry
719 (PTR-MS) medical applications, food control and environmental research,
720 International Journal of Mass Spectrometry and Ion Processes, 173, 191-241,
721 http://dx.doi.org/10.1016/S0168-1176(97)00281-4, 1998.
722 Liu, P. S. K., Deng, R., Smith, K. A., Williams, L. R., Jayne, J. T., Canagaratna, M. R.,
723 Moore, K., Onasch, T. B., Worsnop, D. R., and Deshler, T.: Transmission Efficiency
724 of an Aerodynamic Focusing Lens System: Comparison of Model Calculations and
725 Laboratory Measurements for the Aerodyne Aerosol Mass Spectrometer, Aerosol.
726 Sci. Tech., 41, 721-733, 10.1080/02786820701422278, 2007.
727 Liu, T. Y., Wang, X. M., Wang, B. G., Ding, X., Deng, W., Lü, S. J., and Zhang, Y. L.:
728 Emission factor of ammonia (NH_3) from on-road vehicles in China: tunnel tests in
729 urban Guangzhou, Environ. Res. Lett., 9, 064027, 2014.
730 McFiggans, G., Artaxo, P., Baltensperger, U., Coe, H., Facchini, M. C., Feingold, G.,
731 Fuzzi, S., Gysel, M., Laaksonen, A., Lohmann, U., Mentel, T. F., Murphy, D. M.,
732 O'Dowd, C. D., Snider, J. R., and Weingartner, E.: The effect of physical and
733 chemical aerosol properties on warm cloud droplet activation, Atmos.
734 Chem. Phys., 6, 2593–2649, doi:10.5194/acp-6-2593-2006, 2006.
735 McMurry, P. H., and Grosjean, D.: Gas and aerosol wall losses in Teflon film smog
736 chambers, Environ. Sci. Technol., 19, 1176-1182, 10.1021/es00142a006, 1985.

737 Miracolo, M. A., Presto, A. A., Lambe, A. T., Hennigan, C. J., Donahue, N. M., Kroll,
738 J. H., Worsnop, D. R., and Robinson, A. L.: Photo-oxidation of low-volatility
739 organics found in motor vehicle emissions: Production and chemical evolution of
740 organic aerosol mass, Environ. Sci. Technol., 44, 1638-1643, 10.1021/es902635c,
741 2010.
742 National Bureau of Statistics of China: China Statistical Yearbook, Beijing: China
743 Statistics Press, 2013.
744 Nakao, S., Shrivastava, M., Nguyen, A., Jung, H., and Cocker, D.: Interpretation of
745 Secondary Organic Aerosol Formation from Diesel Exhaust Photooxidation in an
746 Environmental Chamber, Aerosol. Sci. Tech., 45, 964-972,
747 10.1080/02786826.2011.573510, 2011.
748 Ng, N. L., Kroll, J. H., Chan, A. W. H., Chhabra, P. S., Flagan, R. C., and Seinfeld, J.
749 H.: Secondary organic aerosol formation from m-xylene, toluene, and benzene,
750 Atmos. Chem. Phys., 7, 3909-3922, 10.5194/acp-7-3909-2007, 2007.
751 Ng, N. L., Canagaratna, M. R., Zhang, Q., Jimenez, J. L., Tian, J., Ulbrich, I. M.,
752 Kroll, J. H., Docherty, K. S., Chhabra, P. S., Bahreini, R., Murphy, S. M., Seinfeld,
753 J. H., Hildebrandt, L., Donahue, N. M., DeCarlo, P. F., Lanz, V. A., Prévôt, A. S. H.,
754 Dinar, E., Rudich, Y., and Worsnop, D. R.: Organic aerosol components observed in
755 Northern Hemispheric datasets from Aerosol Mass Spectrometry, Atmos. Chem.
756 Phys., 10, 4625-4641, 10.5194/acp-10-4625-2010, 2010.
757 Ng, N. L., Canagaratna, M. R., Jimenez, J. L., Chhabra, P. S., Seinfeld, J. H., and

758 Worsnop, D. R.: Changes in organic aerosol composition with aging inferred from
759 aerosol mass spectra, Atmos. Chem. Phys., 11, 6465-6474,
760 10.5194/acp-11-6465-2011, 2011.
761 Nordin, E. Z., Eriksson, A. C., Roldin, P., Nilsson, P. T., Carlsson, J. E., Kajos, M. K.,
762 Hellén, H., Wittbom, C., Rissler, J., Löndahl, J., Swietlicki, E., Svenningsson, B.,
763 Bohgard, M., Kulmala, M., Hallquist, M., and Pagels, J. H.: Secondary organic
764 aerosol formation from idling gasoline passenger vehicle emissions investigated in
765 a smog chamber, Atmos. Chem. Phys., 13, 6101-6116, 10.5194/acp-13-6101-2013,
766 2013.
767 Odum, J. R., Hoffmann, T., Bowman, F., Collins, D., Flagan, R. C., and Seinfeld, J. H.:
768 Gas/particle partitioning and secondary organic aerosol yields, Environ. Sci.
769 Technol., 30, 2580-2585, 10.1021/es950943+, 1996.
770 Odum, J. R., Jungkamp, T. P. W., Griffin, R. J., Forstner, H. J. L., Flagan, R. C., and
771 Seinfeld, J. H.: Aromatics, reformulated gasoline, and atmospheric organic aerosol
772 formation, Environ. Sci. Technol., 31, 1890-1897, 10.1021/es960535l, 1997.
773 Pankow, J. F.: An absorption-model of gas-particle partitioning of organic compounds
774 in the atmosphere, Atmos. Environ., 28, 185-188, 1994a.
775 Pankow, J. F.: An absorption-model of the gas aerosol partitioning involved in the
776 formation of secondary organic aerosol, Atmos. Environ., 28, 189-193, 1994b.
777 Pathak, R. K., Stanier, C. O., Donahue, N. M., and Pandis, S. N.: Ozonolysis of
778 alpha-pinene at atmospherically relevant concentrations: Temperature dependence

779 of aerosol mass fractions (yields), J Geophys Res-Atmos, 112,
780 10.1029/2006jd007436, 2007.
781 Platt, S. M., El Haddad, I., Zardini, A. A., Clairotte, M., Astorga, C., Wolf, R., Slowik,
782 J. G., Temime-Roussel, B., Marchand, N., Ježek, I., Drinovec, L., Močnik, G.,
783 Möhler, O., Richter, R., Barmet, P., Bianchi, F., Baltensperger, U., and Prévôt, A. S.
784 H.: Secondary organic aerosol formation from gasoline vehicle emissions in a new
785 mobile environmental reaction chamber, Atmos. Chem. Phys., 13, 9141-9158,
786 10.5194/acp-13-9141-2013, 2013.
787 Presto, A. A., Gordon, T. D., and Robinson, A. L.: Primary to secondary organic
788 aerosol: evolution of organic emissions from mobile combustion sources, Atmos.
789 Chem. Phys., 14, 5015-5036, 10.5194/acp-14-5015-2014, 2014.
790 Robinson, A. L., Donahue, N. M., Shrivastava, M. K., Weitkamp, E. A., Sage, A. M.,
791 Grieshop, A. P., Lane, T. E., Pierce, J. R., and Pandis, S. N.: Rethinking Organic
792 Aerosols: Semivolatile Emissions and Photochemical Aging, Science, 315,
793 1259-1262, 10.1126/science.1133061, 2007.
794 Samy, S., and Zielinska, B.: Secondary organic aerosol production from modern
795 diesel engine emissions, Atmos. Chem. Phys., 10, 609-625,
796 10.5194/acp-10-609-2010, 2010.
797 Saxena, P., and Hildemann, L.: Water-soluble organics in atmospheric particles: A
798 critical review of the literature and application of thermodynamics to identify
799 candidate compounds, J. Atmos. Chem., 24, 57-109, 10.1007/BF00053823, 1996.

800 Schauer, J. J., Kleeman, M. J., Cass, G. R., and Simoneit, B. R. T.: Measurement of
801 emissions from air pollution sources. 5. C1−C32 organic compounds from
802 gasoline-powered motor vehicles, Environ. Sci. Technol., 36, 1169-1180,
803 10.1021/es0108077, 2002.
804 Shakya, K. M., and Griffin, R. J.: Secondary organic aerosol from photooxidation of
805 polycyclic aromatic hydrocarbons, Environ. Sci. Technol., 44, 8134-8139,
806 10.1021/es1019417, 2010.
807 Song, C., Na, K., Warren, B., Malloy, Q., and Cocker, D. R.: Impact of Propene on
808 Secondary Organic Aerosol Formation from m-Xylene, Environ Sci Technol, 41,
809 6990-6995, 10.1021/es062279a, 2007.
810 Tkacik, D. S., Presto, A. A., Donahue, N. M., and Robinson, A. L.: Secondary organic
811 aerosol formation from intermediate-volatility organic compounds: cyclic, linear,
812 and branched alkanes, Environ. Sci. Technol., 46, 8773-8781, 10.1021/es301112c,
813 2012.
814 Tkacik, D. S., Lambe, A. T., Jathar, S., Li, X., Presto, A. A., Zhao, Y. L., Blake, D.,
815 Meinardi, S., Jayne, J. T., Croteau, P. L., and Robinson, A. L.: Secondary Organic
816 Aerosol Formation from in-Use Motor Vehicle Emissions Using a Potential Aerosol
817 Mass Reactor, Environ Sci Technol, 48, 11235-11242, 10.1021/es502239v, 2014.
818 Tong, H. Y., Hung, W. T., and Cheung, C. S.: On-road motor vehicle emissions and
819 fuel consumption in urban driving conditions, Journal of the Air & Waste
820 Management Association, 50, 543-554, 2000.

Volkamer, R., Jimenez, J. L., San Martini, F., Dzepina, K., Zhang, Q., Salcedo, D., Molina, L. T., Worsnop, D. R., and Molina, M. J.: Secondary organic aerosol formation from anthropogenic air pollution: Rapid and higher than expected, Geophys. Res. Lett., 33, L17811, 10.1029/2006gl026899, 2006.

Wagner, D. V., An, F., and Wang, C.: Structure and impacts of fuel economy standards for passenger cars in China, Energy. Policy., 37, 3803-3811, doi:10.1016/j.enpol.2009.07.009, 2009.

Wang, J., Jin, L., Gao, J., Shi, J., Zhao, Y., Liu, S., Jin, T., Bai, Z., and Wu, C.-Y.: Investigation of speciated VOC in gasoline vehicular exhaust under ECE and EUDC test cycles, Sci. Total Environ., 445–446, 110-116, http://dx.doi.org/10.1016/j.scitotenv.2012.12.044, 2013.

Wang, X. H., Bi, X. H., Sheng, G. Y., and Fu, J. M.: Chemical composition and sources of PM_{10} and $PM_{2.5}$ aerosols in Guangzhou, China, Environ. Monit. Assess., 119, 425-439, DOI 10.1007/s10661-005-9034-3, 2006.

Wang, X. M., and Wu. T.: Release of isoprene and monoterpenes during the aerobic decomposition of orange wastes from laboratory incubation experiments, Environ. Sci. Technol., 42, 3265-3270, 2008.

Wang, X., Liu, T., Bernard, F., Ding, X., Wen, S., Zhang, Y., Zhang, Z., He, Q., Lü, S., Chen, J., Saunders, S., and Yu, J.: Design and characterization of a smog chamber for studying gas-phase chemical mechanisms and aerosol formation, Atmos. Meas. Tech., 7, 301-313, 10.5194/amt-7-301-2014, 2014.

842 Wehner, B., Wiedensohler, A., Tuch, T. M., Wu, Z. J., Hu, M., Slanina, J., and Kiang,
843 C. S.: Variability of the aerosol number size distribution in Beijing, China: New
844 particle formation, dust storms, and high continental background, Geophys. Res.
845 Lett., 31, L22108, 10.1029/2004GL021596, 2004.
846 Weitkamp, E. A., Sage, A. M., Pierce, J. R., Donahue, N. M., and Robinson, A. L.:
847 Organic aerosol formation from photochemical oxidation of diesel exhaust in a
848 smog chamber, Environ. Sci. Technol., 41, 6969-6975, 10.1021/es070193r, 2007.
849 Yang, H., Yu, J. Z., Ho, S. S. H., Xu, J. H., Wu, W. S., Wan, C. H., Wang, X. D., Wang,
850 X. R., and Wang, L. S.: The chemical composition of inorganic and carbonaceous
851 materials in $PM_{2.5}$ in Nanjing, China, Atmos. Environ., 39, 3735-3749, DOI
852 10.1016/j.atmosenv.2005.03.010, 2005.
853 Yi, Z., Wang, X., Sheng, G., Zhang, D., Zhou, G., and Fu, J.: Soil uptake of carbonyl
854 sulfide in subtropical forests with different successional stages in south China, J.
855 Geophys. Res., 112, D08302, 10.1029/2006JD008048, 2007.
856 Zhang, Q., Worsnop, D. R., Canagaratna, M. R., and Jimenez, J. L.: Hydrocarbon-like
857 and oxygenated organic aerosols in Pittsburgh: insights into sources and processes
858 of organic aerosols, Atmos. Chem. Phys., 5, 3289-3311, 10.5194/acp-5-3289-2005,
859 2005.
860 Zhang, Q., Jimenez, J. L., Canagaratna, M. R., Allan, J. D., Coe, H., Ulbrich, I.,
861 Alfarra, M. R., Takami, A., Middlebrook, A. M., Sun, Y. L., Dzepina, K., Dunlea,
862 E., Docherty, K., DeCarlo, P. F., Salcedo, D., Onasch, T., Jayne, J. T., Miyoshi, T.,

863 Shimono, A., Hatakeyama, S., Takegawa, N., Kondo, Y., Schneider, J., Drewnick,
864 F., Borrmann, S., Weimer, S., Demerjian, K., Williams, P., Bower, K., Bahreini, R.,
865 Cottrell, L., Griffin, R. J., Rautiainen, J., Sun, J. Y., Zhang, Y. M., and Worsnop, D.
866 R.: Ubiquity and dominance of oxygenated species in organic aerosols in
867 anthropogenically-influenced Northern Hemisphere midlatitudes, Geophys. Res.
868 Lett., 34, L13801, 10.1029/2007gl029979, 2007.
869 Zhang, Q., He, K., and Huo, H.: Policy: Cleaning China's air, Nature, 484, 161-162,
870 2012.
871 Zhang, X., Cappa, C. D., Jathar, S. H., McVay, R. C., Ensberg, J. J., Kleeman, M. J.,
872 and Seinfeld, J. H.: Influence of vapor wall loss in laboratory chambers on yields of
873 secondary organic aerosol, Proceedings of the National Academy of Sciences,
874 10.1073/pnas.1404727111, 2014.
875 Zhang, X., Schwantes, R. H., McVay, R. C., Lignell, H., Coggon, M. M., Flagan, R.
876 C., and Seinfeld, J. H.: Vapor wall deposition in Teflon chambers, Atmos. Chem.
877 Phys., 15, 4197-4214, 10.5194/acp-15-4197-2015, 2015.
878 Zhang, Y. L., Guo, H., Wang, X. M., Simpson, I. J., Barletta, B., Blake, D. R.,
879 Meinardi, S., Rowland, F. S., Cheng, H. R., Saunders, S. M., and Lam, S. H. M.:
880 Emission patterns and spatiotemporal variations of halocarbons in the Pearl River
881 Delta region, southern China. J. Geophys. Res., 115, D15309,
882 doi:10.1029/2009JD013726, 2010
883 Zhang, Y., Wang, X., Blake, D. R., Li, L., Zhang, Z., Wang, S., Guo, H., Lee, F. S. C.,

884 Gao, B., Chan, L., Wu, D., and Rowland, F. S.: Aromatic hydrocarbons as ozone
885 precursors before and after outbreak of the 2008 financial crisis in the Pearl River
886 Delta region, south China, J. Geophys. Res., 117, D15306, 10.1029/2011JD017356,
887 2012.
888 Zhang, Y., Wang, X., Zhang, Z., Lü, S., Shao, M., Lee, F. S. C., and Yu, J.: Species
889 profiles and normalized reactivity of volatile organic compounds from gasoline
890 evaporation in China, Atmos. Environ., 79, 110-118,
891 http://dx.doi.org/10.1016/j.atmosenv.2013.06.029, 2013.
892 Zhang, Y. L., Wang, X. M., Li, G. H., Yang, W. Q., Huang, Z. H., Zhang, Z., Huang, X.
893 Y., Deng, W., Liu, T. Y., Huang, Z. Z., and Zhang, Z. Y.: Emission factors of fine
894 particles, carbonaceous aerosols and traces gases from road vehicles: recent tests in
895 an urban tunnel in the Pearl River Delta, China, Atmos. Environ., in review, 2015.
896

897 **Table 1.** Detailed information of the two light-duty gasoline vehicles.

ID	Emission standard class	Vehicle	Model year	Mileage (km)	Displacement (cm^3)	Power (kW)	Weight (kg)
Ⅰ	Euro4	Golf	2011	25000	1598	77	1295
II	Euro1	Accord	2002	237984	2298	110	1423

898

899

900 **Table 2.** Initial conditions for the light-duty gasoline vehicle photooxidation

901 experiments.

Experiment #	Vehicle ID	T (℃)[a]	RH (%)[a]	VOC/ NO_x	VOCs (ppbv)[b]	NO (ppbv)	NO_2 (ppbv)
1	Ⅰ	25.8±0.7	52.0±1.8	10.2	1368	115.1	18.4
2	II	24.1±0.6	57.0±2.0	6.0	2583	431.0	0.6
3	Ⅰ	25.0±0.8	52.9±2.0	9.3	2896	300.6	9.5
4	Ⅰ	24.2±0.8	52.5±2.7	2.0	1885	794.1	161.9
5	II	25.0±0.3	52.6±1.3	7.2	1507	210.4	0.7

902 [a]: Stated uncertainties (1σ) are from scatter in temperature and relative humidity, respectively.

903 [b]: C2-C3 and C4-C12 hydrocarbons were measured by GC-FID and GC-MSD, respectively.

904 **Table 3.** Summary of the results for the light-duty gasoline vehicle photooxidation

905 experiments.

Exp #	Vehicle ID	OH ($\times 10^6$ molecules cm^{-3})	POA ($\mu g\ m^{-3}$)	SOA ($\mu g\ m^{-3}$)	SOA/POA	Effective yield
1	I	1.23	1.1	51.1	46	0.103
2	II	0.73	0.2	17.6	88	0.038
3	I	0.88	0.3	77.6	259	0.119
4	I	1.20	1.0	125.4	125	0.172
5	II	0.79	0.3	4.0	12	0.028

906

907

908

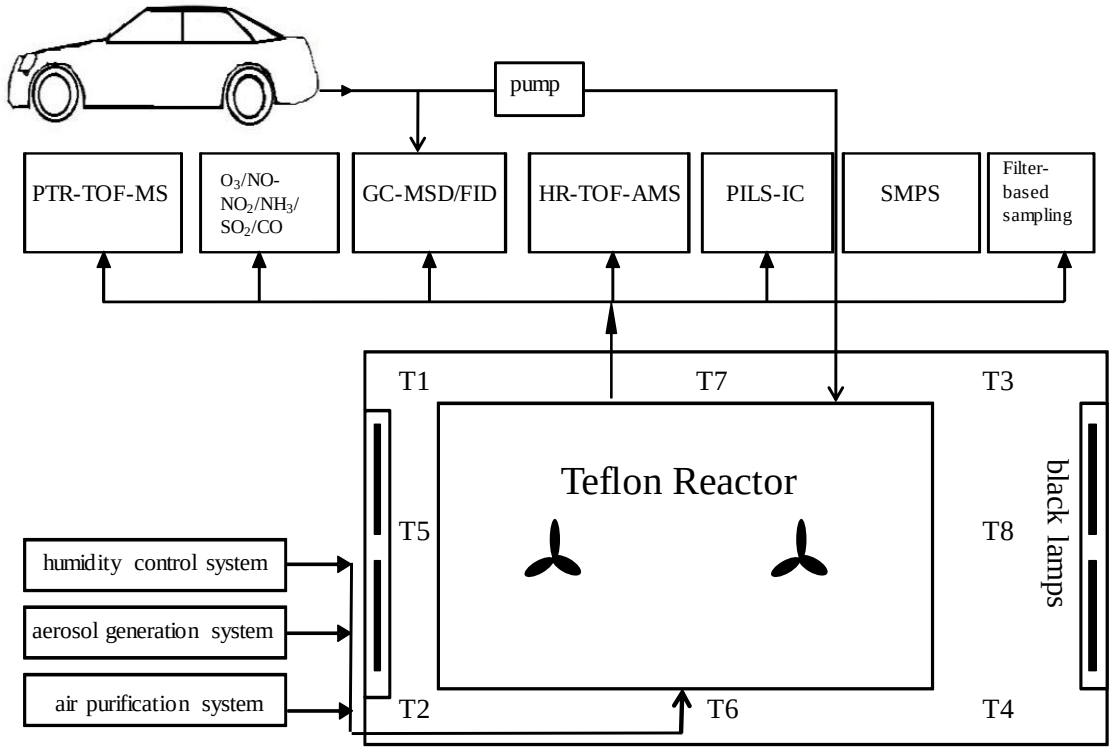

Fig. 1. Schematic of the GIG-CAS smog chamber facility and vehicle exhaust injection system.

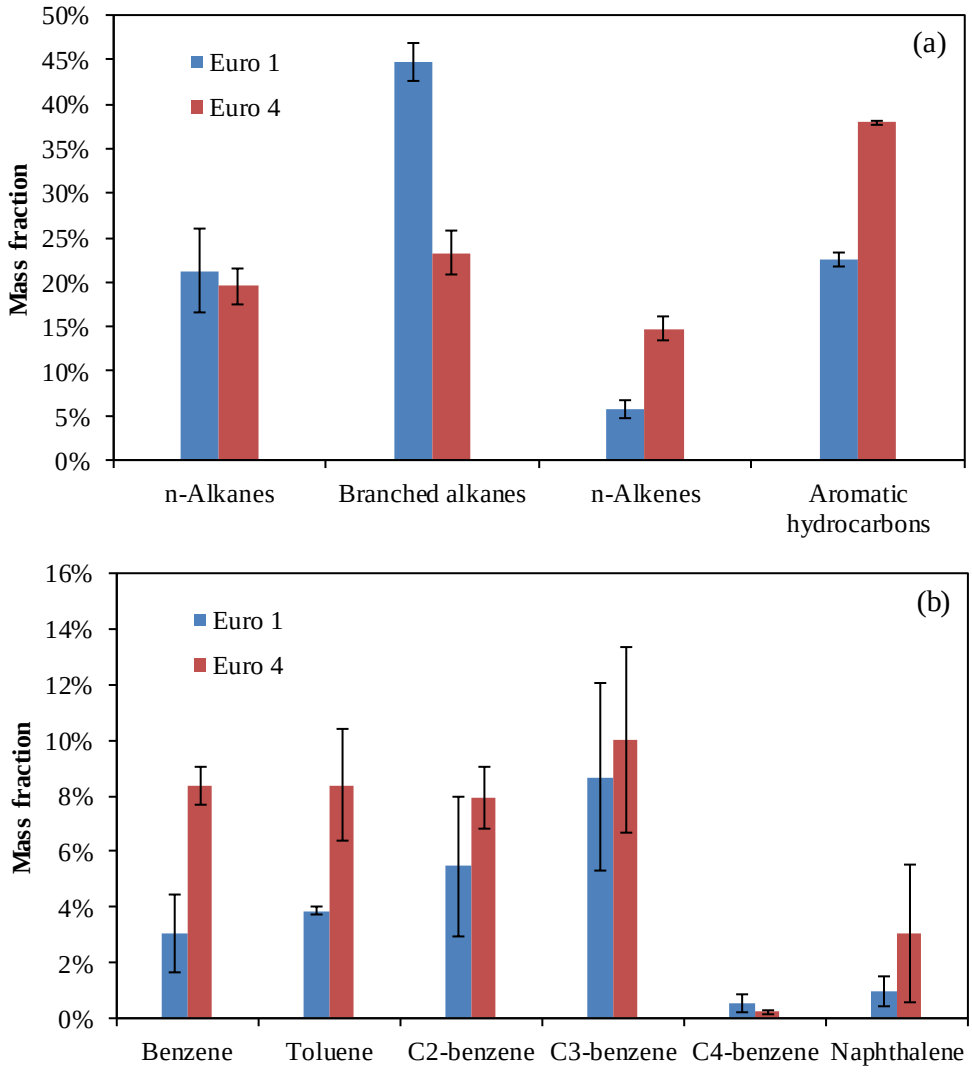

Fig. 2. Composition of **(a)** VOCs and **(b)** aromatics of gasoline vehicle exhausts from Euro 1 and Euro 4 private cars, presented as weight percentage of speciated VOCs. C2-C3 and C4-C12 hydrocarbons were measured by GC-FID and GC-MSD, respectively. The error bars (1 σ) represent variability from measurements for each vehicle.

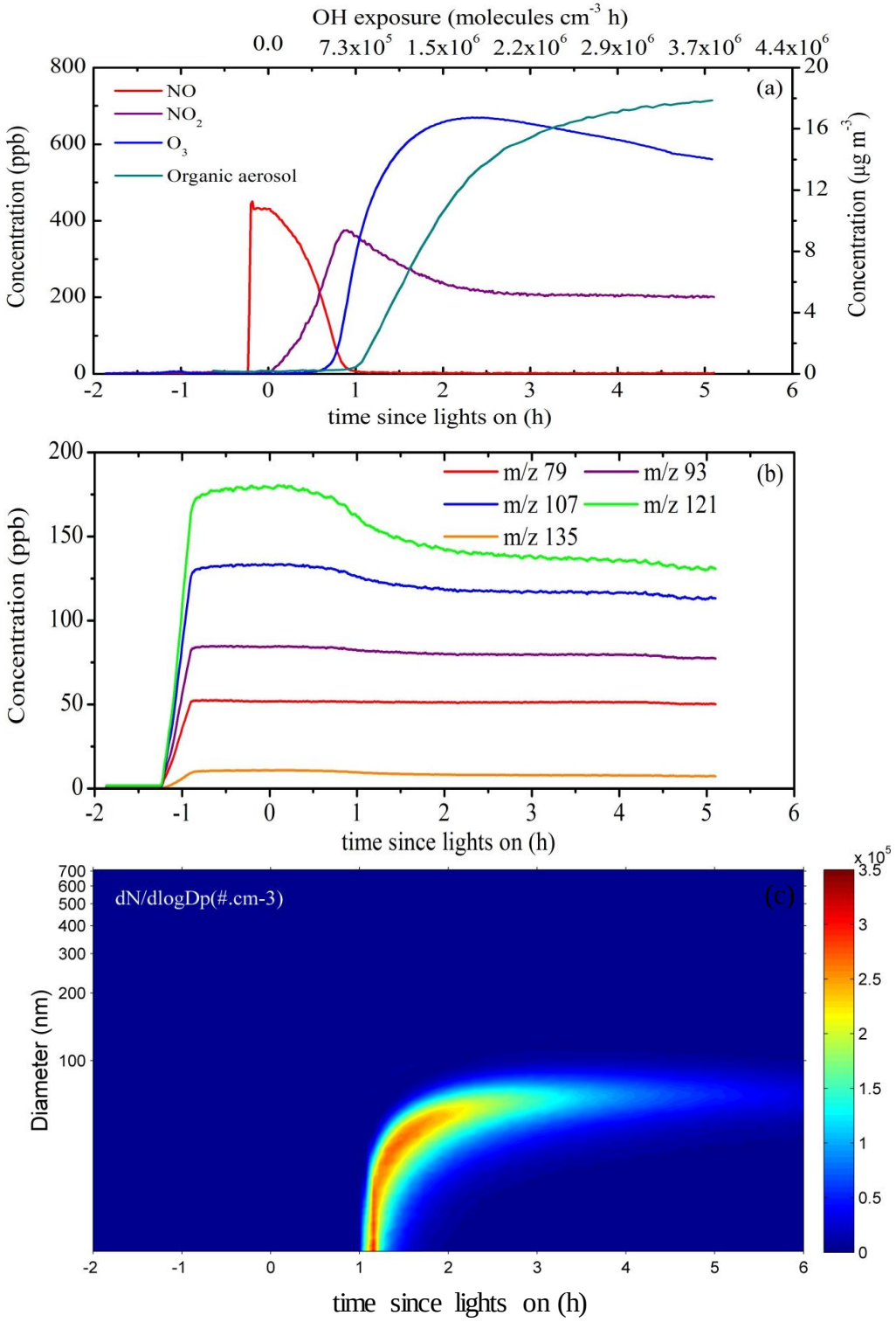

921

922 **Fig. 3**. Concentration–time plots of gas–phase and particle–phase species and particle
923 number concentration distribution as a function of time during a typical smog
924 chamber experiment (experiment 2): **(a)** NO, NO_2, O_3 (left *y* axis) and organic aerosol
925 (right *y* axis); **(b)** gas-phase light aromatics (measured by PTR-TOF-MS) (benzene

characterized by m/z 79; toluene characterized by m/z 93; C_2–benzene characterized by m/z 107; C_3–benzene characterized by m/z 121; C_4-benzene characterized by m/z 135); **(c)** particle size-number concentration distributions as a function of time. The vehicle exhaust was introduced into the reactor between -1.3 h and -0.85 h; the primary emissions were characterized from -0.85 h to 0 h; at time = 0 h, the black lamps were turned on.

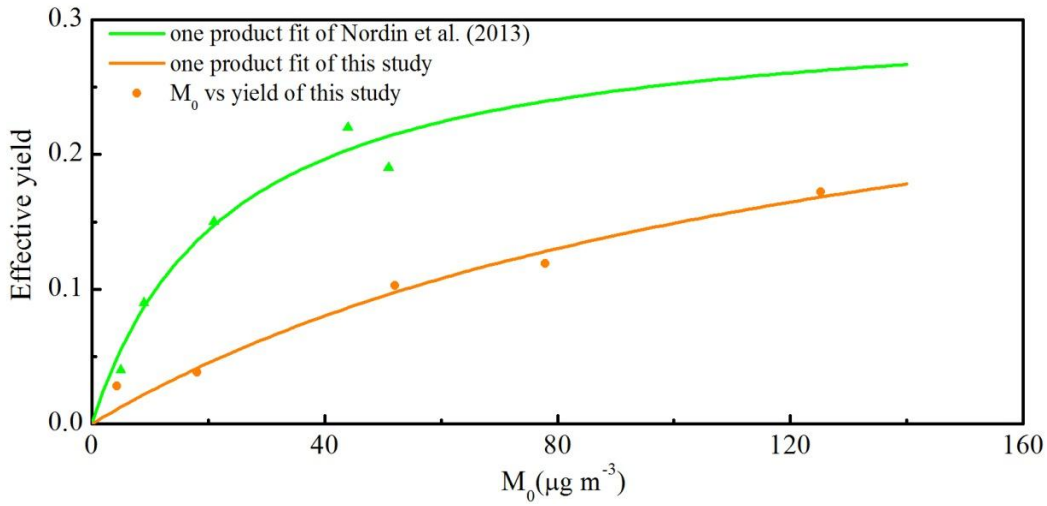

Fig. 4. Comparison of yield data obtained for the gasoline experiments in this study with that of Nordin et al. (2013). The green line is the best fit one-product model (α_1 = 0.311, $K_{om,1}$ = 0.043) for the data set of Nordin et al. (2013). The orange line is the best one-product fit to the effective SOA yield in this study (α_1 = 0.350, $K_{om,1}$ = 0.007). Organic precursors in the calculation of effective yields included benzene, toluene, C2–benzene, C3–benzene, C4-benzene and naphthalene.

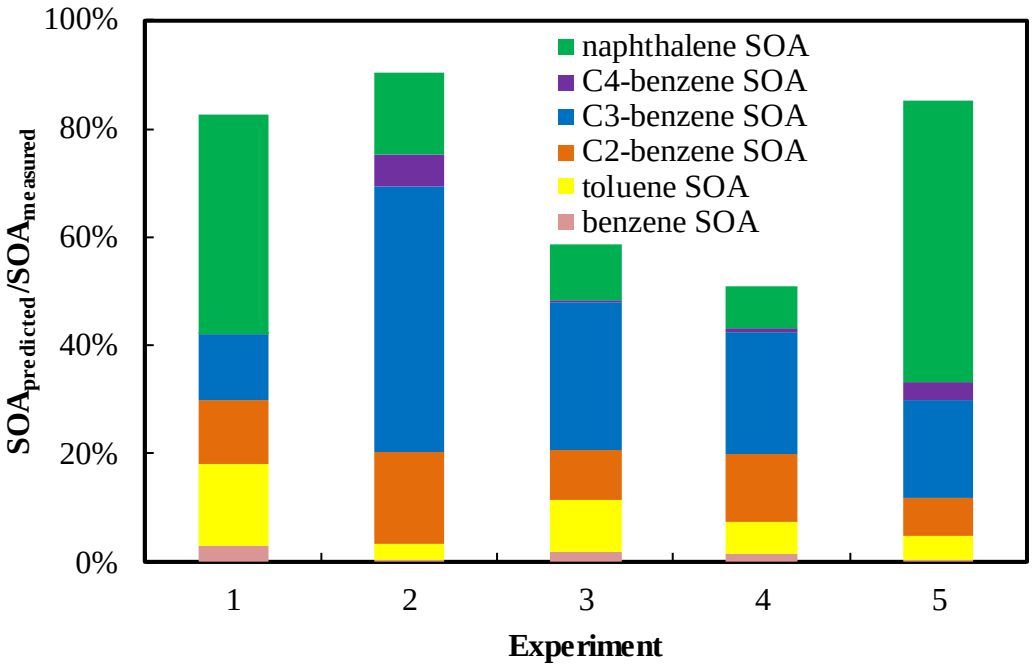

941

942 **Fig. 5**. Contributions of the predicted benzene SOA, toluene SOA, C2–benzene SOA,

943 C3–benzene SOA, C4–benzene SOA and naphthalene SOA to the total formed SOA

944 in all experiments.

945

946

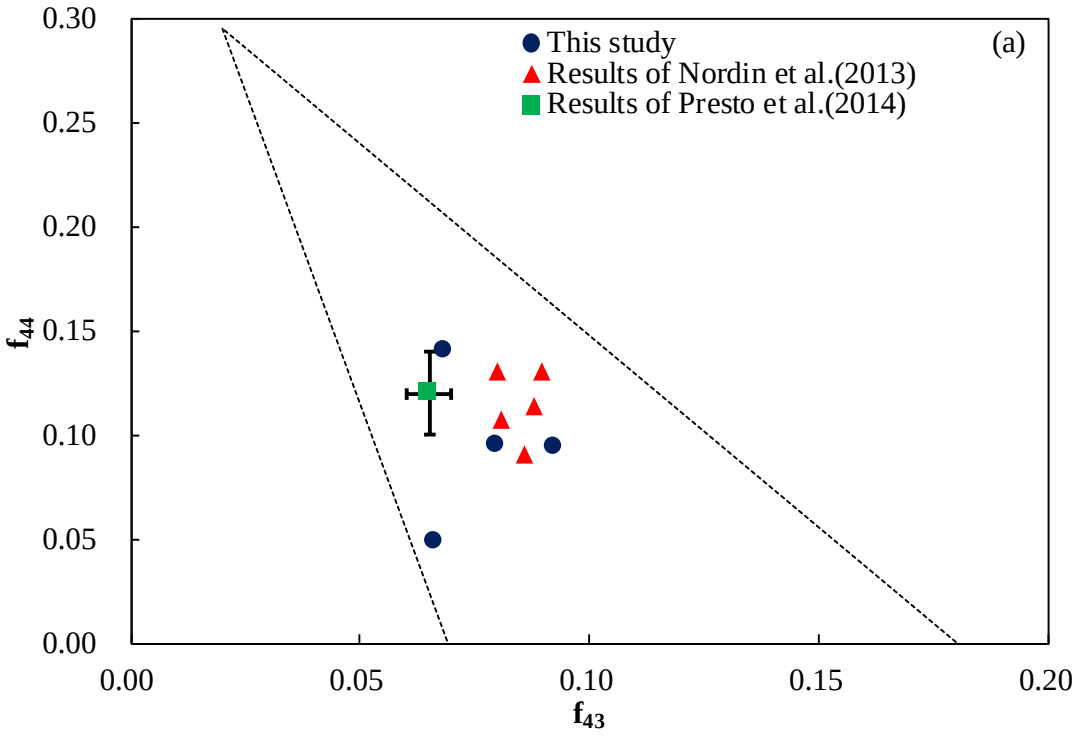

947

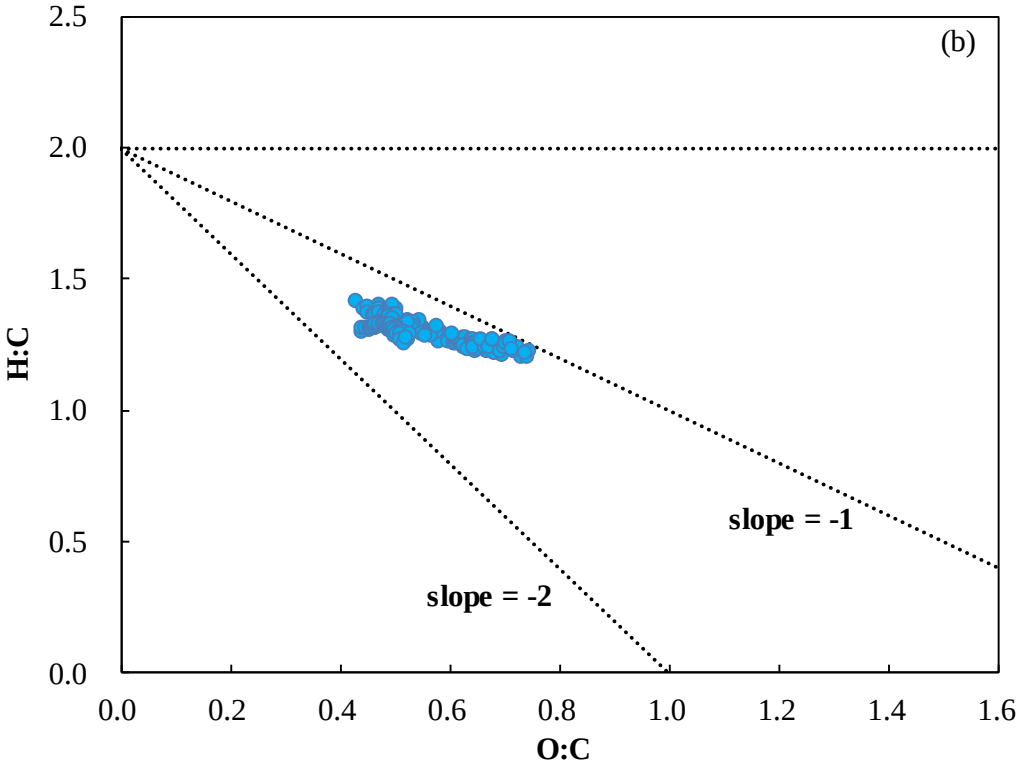

948

949 **Fig. 6**. **(a)** The fractions of total organic signal at m/z 43 (f_{43}) vs. m/z (f_{44}) at the end
950 of each experiment together with the triangle plot of Ng et al. (2010). The solid square
951 and triangles represent the results of Presto et al. (2014) and Nordin et al. (2013),
952 respectively. The dotted lines define the space where ambient OOA components fall.

The ranges of f_{44} observed for SV-OOA and LV-OOA components are 0.03–0.11 and 0.13–0.21**,** respectively. **(b)** Van Krevelen diagram of SOA from light-duty gasoline vehicle exhaust. Dotted lines are to show slopes of 0, -1 and -2. AMS data of the experiment 5 were unavailable.